IEEE Access
Multidisciplinary ⋮ Rapid Review ⋮ Open Access Journal

Received 29 February 2024, accepted 13 March 2024, date of publication 21 March 2024, date of current version 27 March 2024.

Digital Object Identifier 10.1109/ACCESS.2024.3380475

RESEARCH ARTICLE

New Global Maximum Power Point Tracking Technique Based on Indirect PV Array Voltage Control for Photovoltaic String Inverters With Reduced Number of Sensors

PEDRO A. R. FREITAS[1], LUCAS P. PIRES[2], LUIZ C. FREITAS[3], ÊNIO C. RESENDE[3], HENRIQUE T. DE M. CARVALHO[3], LUIZ C. G. FREITAS[3], AND GUSTAVO B. LIMA[3]

[1]Department of Electrical Engineering, Federal Institute of the Triângulo Mineiro, Campus Patrocínio, Patrocínio, Minas Gerais 38747-792, Brazil
[2]Department of Electrical Engineering, Federal University of Triângulo Mineiro, Uberaba, Minas Gerais 38025-180, Brazil
[3]Faculty of Electrical Engineering, Federal University of Uberlândia, Campus Santa Monica, Uberlândia, Minas Gerais 38400-902, Brazil

Corresponding author: Luiz C. G. Freitas (lcgfreitas@ufu.br)

This work was supported in part by the Federal University of Uberlândia (UFU); in part by Conselho Nacional de Desenvolvimento Científico e Tecnológico (CNPq) under Grant 314353/2021-6, Grant 407403/2022-1, and Grant 406881/2022-7; in part by Fundação de Amparo à Pesquisa do Estado de Minas Gerais (Fapemig) under Grant APQ-04929-22; and in part by Coordenação de Aperfeiçoamento de Pessoal de Nível Superior (CAPES)—Finance Code 001.

ABSTRACT This paper presents a study regarding the development of a single-stage single-phase grid-tied photovoltaic (PV) inverter with a new Global Maximum Power Point Tracking (GMPPT) technique. The proposed strategy is based on the indirect PV array voltage control and allows for the development of PV inverter with reduced number of sensors, therefore, increasing the system reliability and reducing costs. The proposed strategy was denominated Sensorless PV Array Voltage Control for Global Maximum Power Point Tracking (SPVAVC-GMPPT). The static and dynamic accuracy of the GMPPT algorithm has been demonstrated to be over 99% under different operating conditions of irradiance and temperature and also under shading conditions, where multiple false Maximum Power Points (MPPs) occur. Simulation and experimental results are shown, compared, and discussed, with a 99,45% TF for standard-test conditions (STC – 25 °C and 1000 W/m^2) and even higher (99,96%) under different irradiance and temperature proving the effectiveness of the proposed technique.

INDEX TERMS GMPPT, grid-tied inverters, photovoltaic systems, sensorless.

I. INTRODUCTION

In recent decades, with the trend of reducing fossil fuel supply coupled with concerns about environmental impact, investments in renewable energy research have intensified. In this context, photovoltaic energy has gained strong prominence due to its inexhaustible primary source, and the search for grid-tied photovoltaic (PV) inverters with highly efficient Global Maximum Power Point Tracking (GMPPT) techniques has become a topic of many studies [1], [2], [3], [4], [5].

In classical GMPPT techniques, typically 4 to 5 sensors are used for system control, usually including two voltage sensors and two current sensors: voltage and current of the PV array, DC bus voltage, grid voltage, and filter inductor current [4].

In [6], the authors discuss the challenges faced by traditional MPPT algorithms due to dynamic irradiance change, highlighting the importance of developing improved GMPPT algorithms for better tracking performance under partial shading conditions. In this context, they propose a hybrid

The associate editor coordinating the review of this manuscript and approving it for publication was Inam Nutkani.

control combining an artificial neural network (ANN) and an augmented state feedback precise linearization (AFL) controller with fast response to dynamic irradiance change.

In [7], the authors analyze 45 published works focused on soft computing MPPT techniques such as Artificial Bayesian network and chaotic search, which are fast and efficient techniques, but with high complexity.

In [8], the authors compare one hundred and thirty-nine papers (139) of MPPT strategies developed based on Artificial Intelligence (AI) and the performance of MPPT strategies based on Artificial Neural Network are all presented and evaluated under uniform and non-uniform irradiance conditions (shading and partial shading). The tracking accuracy was above 99% with fast convergence speed however, the complex calculations involved result in high computational requirements.

In [9], one hundred and nine works (109) involving classical MPPT techniques (P&O-Perturb and Observe, Incremental Conductance, Hill Climbing, etc.) including hybrids with AI-based optimization were evaluated and compared in terms of efficiency, number of sensors, convergence speed, and application (off-grid and on-grid systems) under shading and partial shading conditions. Some of these techniques were considered as simple, but proved to fail under unusual cases of shading. Others, considered immune to partial shading conditions, needed multiple sensors and had complex algorithms, consequently increasing both signal processing requirements and costs.

In [10], the authors analyze and compare 40 different MPPT techniques, and some of them can be highlighted for their algorithm simplicity, such as linear current control and the only-current PV. In [11], the authors analyzed fifty-eight (58) studies and conducted the analyses not only on performance (tracking accuracy, convergence speed, steady state oscillation), but also on economic benefits (algorithm complexity, number of sensors, microcontrollers).

Other works focus on specific studies of one single GMPPT technique. Reference [12] proposes a fuzzy improve to hill –climbing search method, achieving a high efficient GMPPT strategy, but also with high complexity and cost. Less complex controls are presented in many other papers [13], [14], [15] but with less GMPPT reliability and, even these, also uses 4 sensors or more. Finally, in [16] the authors discuss how the use of excessive sensors can have a negative impact on system reliability and increases costs, especially current sensors, which are usually shunt resistors or Hall Effect sensors.

In this context, in [17] the authors presented a study concerning the design and development of a grid-tied PV inverter with GMPPT technique and reduced number of sensors. The proposed GMPPT technique can be understood as an indirect control method of the PV array voltage (VPV). It was demonstrated that imposed modifications (perturbances) on the PV inverter's output current (current injected into the grid) leads to another on the PV inverter's input voltage (VPV). Thus, one must note that changes in the environmental parameters such as temperature and irradiance changes input power that can be provided by the PV array and leads to different operational points, consequently bringing the need for changes in current injected into the grid so that stability is maintained, and operation is given at the MPP. This operating principle allows us to conclude that it is enough to cause changes in the injected current for the PV array to operate naturally at the MPP, eliminating the need for voltage and current sensors on its terminals. In order to achieve this goal, two subroutines were designed, one to calculate the ac power variation and determine the necessary disturbance level to be applied to the injected current reference signal, and another to calculate the necessary peak value of the injected current reference signal to be applied as an input for the PRes (Proportional Resonant) controller chosen as the internal current loop compensator for the PV inverter implementation. That being sad, it is important to highlight that the static and dynamic accuracy of the MPPT algorithm has been demonstrated to be around 99% under different operating conditions of irradiance and temperature, however, the complexity of the proposed control strategy can be considered high. In addition, under shading conditions, where multiple false power point occurs, additional control routine was added to full scanning the output power curve so that the GMPP can be reached, adding another level of complexity to the control system. Despite the improvements achieved by the authors for full scanning of the AC power, losses in the energy harvest are still caused during the scan.

In order to overcome these disadvantages and to advance the research, in this paper the authors are presenting a new algorithm for GMPPT. As well as presented in [17], the algorithm proposed herein can be understood as an indirect control method of the PV array voltage. However, the new algorithm does not require full scanning of the output power curve so that the GMPP can be reached and does not require subroutines to determine the desired injected current reference, reducing both the complexity of the control strategy and the losses in the energy harvest. In addition, a simplified control strategy for the PV inverter could be implemented, as detailed described in this paper. The proposed strategy was denominated as Sensorless PV Array Voltage Control for Global Maximum Power Point Tracking (SPVAVC-GMPPT).

To organize and demonstrate the effectiveness of the proposed solution, the remaining sections of this paper are presented in the following sequence. In Section II a system overview is presented, and the main characteristics of the power structure and the control strategy are described. Detailed explanation of the proposed technique, including flowcharts and discussions of key points are presented in Section III. Simulation and experimental results are shown, compared, and discussed in Section IV. Finally, concluding remarks and closing discussions are presented in Section V.

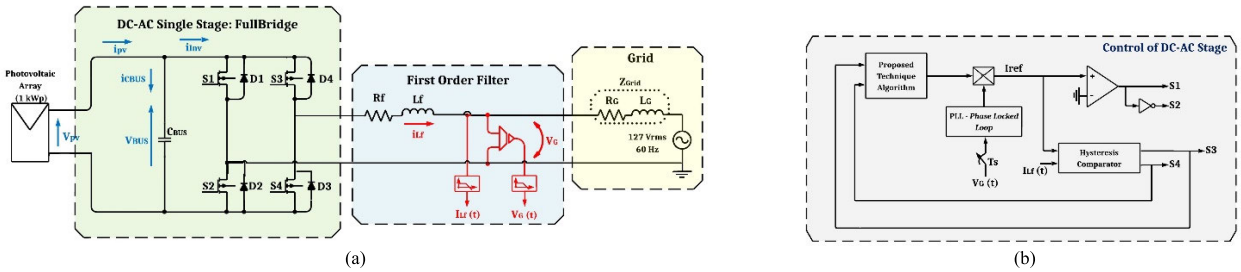

FIGURE 1. Grid-tied single-phase single-stage PV inverter implemented using software PSIM®: (a) power structure (b) control scheme of the SPVAVC-GMPPT technique implemented with digital signal processor TMS320F28335 from Texas Instruments.

II. SYSTEM DESCRIPTION

Figure 1 shows the power and control structure used. Figure 1(a) shows a grid-tied DC–AC single-phase single-stage PV system with a first order filter L_f for grid coupling. The classic single-phase Full-Bridge inverter is responsible for imposing the reference current through the L_f coupling inductor. The current reference imposed is defined and controlled by the proposed technique algorithm. It is worth noting that the choice of a single-stage and single-phase PV system connected to ground allowed not only the reduction of the classic DC-DC converter (input-stage) required for raising the DC-bus voltage, reducing costs and increasing system reliability [18], but also provides an easy solution to the issue of parasitic capacitances by creating a path for it to discharge parasitic current directly to the ground [19].

Figure 1(b) shows the simplified control strategy structure. It shows that the V_G (grid voltage) signal is only used for PLL (Phase Locked Loop) synchronization in order to generate the current reference (I_{ref}) signal in phase with grid voltage by multiplying its sinusoidal output by current amplitude imposed by the technique algorithm. A low frequency switching leg (S1 and S2) is controlled by a half-cycle identification. A hysteresis comparison of I_{ref} and $I_{Lf}(t)$ controls the high frequency switching leg (S3 and S4). Both signals from the high frequency switches (S3 and S4) are used for the technique algorithm in the decisions for the adjustment of I_{ref}.

III. PROPOSED SPVAVC-GMPPT TECHNIQUE

A. BASIC MATHEMATICAL ANALYSIS

From the mathematical analysis of the system's power structure, it is possible to achieve a better understanding of the developed control strategy. Firstly, assuming an ideal system, it can be written:

$$p_{input}(t) = p_{output}(t) \tag{1}$$

where:

$p_{input}(t)$ – Input power [W];

$p_{output}(t)$ – Output power [W];

From the analysis of the circuit loops represented in Figure 1, it is possible to write (2) and (3), describing the input and output powers in terms of the voltage and current parameters and considering unity power factor (only active power is required):

$$p_{input}(t) = v_{pv}(t).i_{pv}(t) \tag{2}$$

$$p_{output}(t) = v_{grid}(t).i_{Lf}(t) \tag{3}$$

where:

$v_{pv}(t)$– Instantaneous voltage of the PV array [V];

$i_{pv}(t)$– Instantaneous current of the PV array [A];

$v_{grid}(t)$– Instantaneous voltage at the grid [V];

$i_{Lf}(t)$ – Instantaneous current injected in the grid [A];

Hence, expanding (1) based on (2) and (3):

$$v_{pv}(t)i_{pv}(t) = v_{grid}(t).i_{Lf}(t) \tag{4}$$

Finally, analyzing (4) and Figure 1, it can be noted that the variables related to power transfer in the proposed topology are: $v_{Bus}(t)$, $i_{inv}(t)$, $i_{pv}(t)$, $i_{CBus}(t)$, $i_{Lf}(t)$ and $v_{grid}(t)$. Only the last variable, $v_{grid}(t)$, is considered as fixed RMS value for this analysis, while all the others are subject to variation and, therefore, control. In this paper the control is based on the imposition of the current injected into the grid ($i_{Lf}(t)$).

Observing (4), variations in the injected grid current affect the dynamics of the circuit, which will react to maintain power balance. In a preliminary analysis, an increase or decrease in $i_{Lf}(t)$ has the same effect on the variables v_{PV} and i_{pv} on the left side of the equation (directly proportional). Assuming a constant RMS grid voltage, when i_{Lf} increases, the system's output power also increases, consequently increasing the power demand at the PV input. As long as the array can provide this power, v_{PV} tends to decrease, and i_{pv} tends to increase, both seeking the MPP, thus indirectly controlling the DC-bus voltage of the system by imposing the current injected into the grid.

It is important to know that, when the power demand at the output exceeds what the PV array can provide at the input, an increase in i_{Lf} will cause an increase in i_{CBus} as the capacitor momentarily tries to provide the additional demanded power. In this process, the capacitor voltage, and consequently V_{Bus}, begins to decrease more rapidly. This process can lead the system to what is called Fast Power Reduction Zone (FPRZ) [17], illustrated in Figure 2, and a correction in the injected current reference must be performed, as will be explained next.

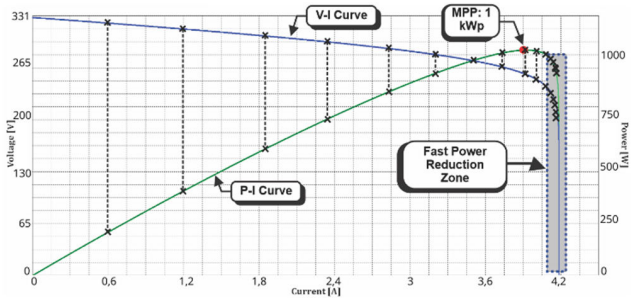

FIGURE 2. I-V and P-V curves illustrating the Fast Power Reduction Zone (FPRZ).

B. GMPPT PRINCIPLES

The flowcharts portrayed in Figures 3 and 4 are used to explain the algorithm developed for the execution of the proposed SPVAVC-GMPPT technique. Figure 3 shows the technique strategy with cyclic perturbation of the main control variable, the injected current reference (I_{ref}). The only sensed variables are the inductor current (i_{Lf}) and the grid voltage (V_g), this last one necessary for grid synchronization. The chosen PLL (Phase Locked Loop) was the Second Order General Integrator (SOGI) due achieving small phase error and a short settling time for single-phase systems, responding quickly to common phase, frequency, and amplitude variations in grid-connected PV systems [20].

The control strategy continuously increments I_{ref} in order to seek the MPP of the PV array, as presented in blocks {5}–{8} (Figure 3). In classical P&O technique, this increment, also known as perturbation, is applied to the V_{Bus} reference. Here, the reference to be incremented is the current injected into the grid. Starting with a low initial value, each increment in the injected current reference (I_{ref}) brings the system closer to the MPP. When I_{ref} surpasses the MPP current, the high-frequency switch (S3 or S4) remains closed for a long period.

In Figure 3, throughout the process, a timer counts the closed time of switches S3 and S4 presented at block {5}, acting as a step definition for the perturbation. As long as the timer does not exceed the predetermined threshold, the current reference continues to be incremented in search of the MPP. When the counter exceeds the threshold, it indicates that the ideal injected current value has been exceeded, and the reference is adjusted to a lower value, as presented at block {9}. Since this reference adjustment is made in order to avoid FPRZ, it is more intense than the cyclic perturbation presented in {8}. This lower value is sustained just enough to recover the DC-bus voltage (V_{Bus}). Then, the reference is increased in order to return close to MPP reference, as presented in blocks {10} and {11}.

The threshold for switch closed time, referred as the correction threshold, can be defined by (7), observing that V_{Bus} and V_{MP} (PV array voltage at MPP) are equal. Hence:

$$V_{Lf} = L_f . di_{Lf}/dt \tag{5}$$

$$V_{MP} - V_{grid} = L_f . di_{Lf}/dt \tag{6}$$

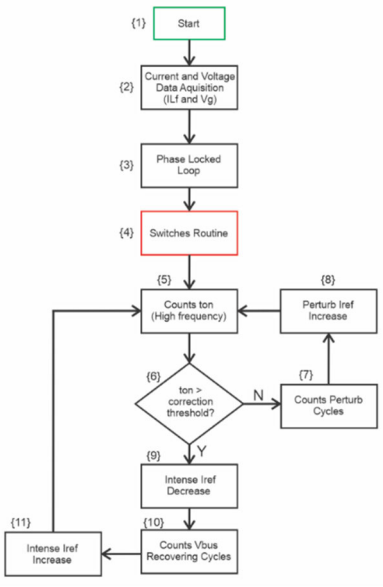

FIGURE 3. Flowchart of the algorithm designed for the implementation of proposed SPVAVC-GMPPT technique.

where:

V_{Lf} - inductor voltage [V];

L_f - inductance [H];

di_{Lf}/dt - inductor current variation [A/s];

Considering the threshold conditions for the closed time of the high frequency switches, it can be written:

$$\Delta t = \frac{L_f \, \Delta i_{Lf}}{V_{MP} - V_{grid}} \tag{7}$$

where:

Δt - high frequency switching period threshold [s];

Δi_{Lf} - current ripple [A]

V_{MP} - maximum power point voltage [V];

To determine the High Frequency Switching Period Threshold (HFSPT), (7) is applied with the projected parameters. In other words, the control logic should decrease the injected current reference if the high-frequency switch remains closed more time than the maximum it would for the MPP. This maximum time occurs at the peak current, and by estimating values for V_{Bus}, V_{grid}, and designing Lf to an acceptable Δi_{Lf} for the hysteresis current controller, the corresponding Δt for the correction of the threshold can be estimated. It is important to highlight that, since only two sensors at the inverter's output are used, the capacitor deployed on the DC-bus will provide the power that the PV array cannot supply during short periods of time when the injected current reference becomes higher than the MPP current. This can result in a significant drop on the DC-bus voltage.

Figure 4 presents the strategy for controlling the switches in the single-stage inverter, referred to Figure 3 as the block {4} "Switches Routine", in which S1 and S2 are controlled with low frequency, with its common point connected to the

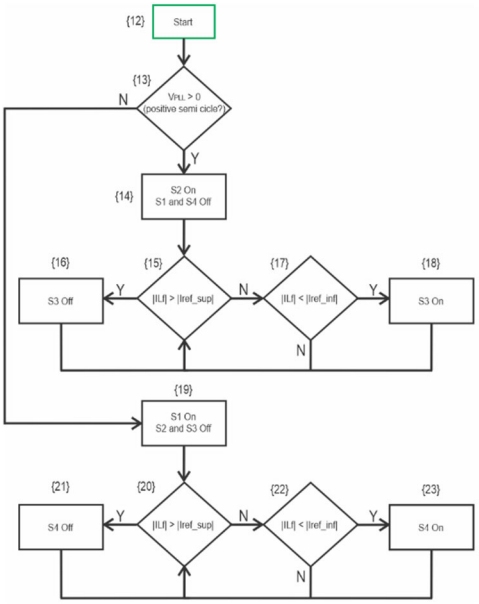

FIGURE 4. Flowchart of the algorithm designed for the generation of the inverter's gate-drive signals.

system's ground. Their switching control is based on half cycle analysis of the PLL reference, as shown in blocks {13}, {14} and {19}, illustrated in Figure 4. Furthermore, S3 and S4 are controlled with high frequency using a hysteresis current controller, imposing the current to be injected into the grid within the limits set by the hysteresis reference (Figure 4, blocks {14}-{18} for positive half cycle and {19}-{23} for negative half cycle).

To exemplify what has just been explained, Fig. 5 shows the behavior of the aforementioned variables obtained through computational simulations. The adjusted values were defined in accordance with the PV inverter design specifications. Analyzing Fig. 5(a), one can note that every 10 cycles the peak value of the injected current reference is increased by 250 mA, analogous to what is done for the PV array voltage with a classical P&O technique. While any of the high-frequency switches remain closed (S_3 or S_4), the time is counted until it opens, resetting it when it does. As observed in Fig.5(b), if this time exceeds the value determined by the defined correction threshold (Ton > HFSPT), the correction Flag is triggered, and the injected current reference (Iref) is decreased by 1.0A. This intense reduction is necessary to avoid huge voltage sag across the DC-bus, so the capacitor voltage (V_{Bus}) can be recovered rapidly, as portrayed in Fig.7. After 5 cycles at this lower value, the injected current reference is increased by 750 mA, taking the system towards the ideal operating point (MPP) again. Under steady-state conditions, the control keeps in this routine, ensuring high Tracking Factor (TF > 99%) for any condition of irradiance and temperature.

Also in Fig.5(b), it can be seen a situation where the correction Flag appears twice in close proximity, despite that, one can observe that the control system is protected against multiple undesired corrections. To achieve this, the command to reduce the injected current reference can only occur again after at least one increase has taken place, thus avoiding system instability.

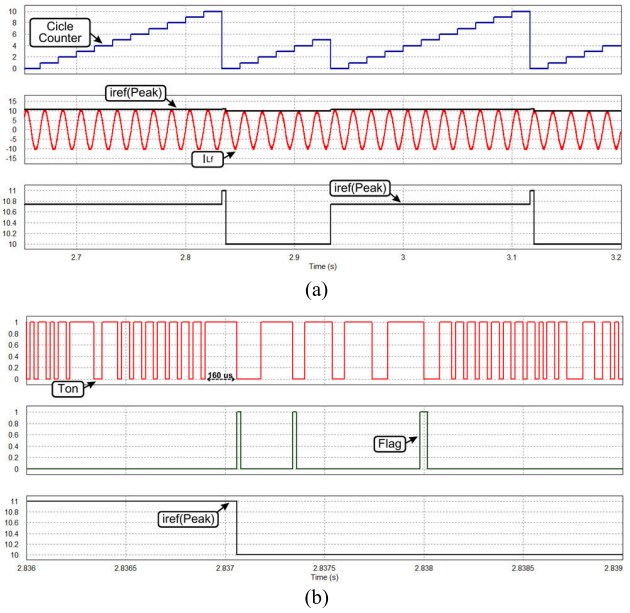

FIGURE 5. Process of injected current reference perturbation: (a) grid cycle counter, serving as a definition of the disturbance step, current injected into the grid (I_{Lf}), injected current reference (I_{ref}); (b) detail of Fig. 5(a) illustrating the moment in which Ton > HFSPT and the correction Flag (FLAG) is triggered so that the injected current reference (I_{ref}) is reduced, avoiding voltage sag on the DC-bus.

C. PV ARRAY VOLTAGE PREDICTION

To guarantee that the GMPPT technique is able to achieve TF >99% under partial shading conditions, the HFSPT must present an adaptive behavior capable of following the PV array voltage variations. To achieve this goal, a current derivative calculation strategy is implemented, and the DC-bus voltage behavior is predicted, as described in the flowchart shown in Figure 6. Firstly, the same input variables described in the previous flowcharts are acquired, as shown in block {25} (Figure 6). Then, the process of calculating the derivative of the injected current is performed, and the estimated DC-bus voltage is calculated, as represented in block {26} and detailed from (8) to (10), described in sequence. One should note that V_{Bus} equals V_{Cap} in the flowchart.

Afterward, in Figure 6 it is verified in which operating range V_{Cap} is located (blocks {27} to {30}) to avoid inappropriate decisions for transient operating conditions, a timer for that range is initiated (blocks {31};{34};{37};{40}), which, if maintained within the same range for a few seconds (to avoid transient conditions to compromise steady state behavior), alters the HFSPT (blocks {33};{36};{39};{42}). The process loops to continually assess the V_{Cap} voltage level under steady-state operation, always seeking the ideal HFSPT for it. Figure 7 illustrates the comparison between the real

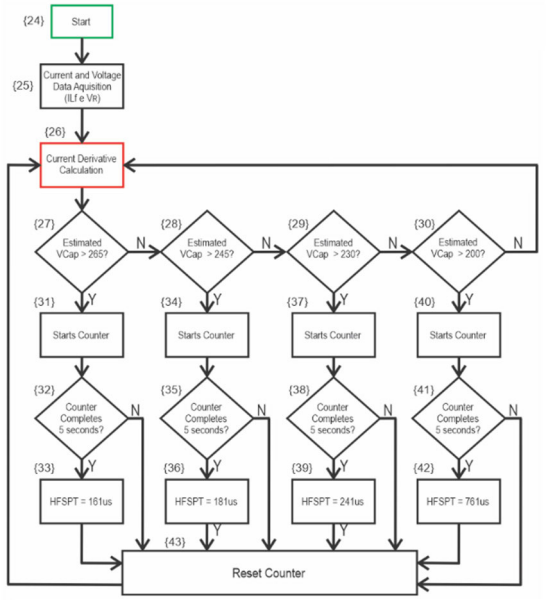

FIGURE 6. Flowchart of the algorithm designed for the correction of the High Frequency Switching Period Threshold (HFSPT).

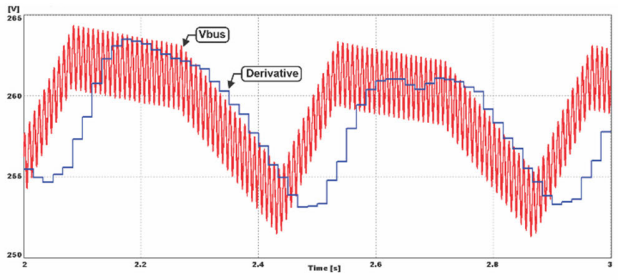

FIGURE 7. DC-bus voltage (V_{Bus}) behavior during injected current reference perturbation: comparison between the measured (red) and calculated values (blue).

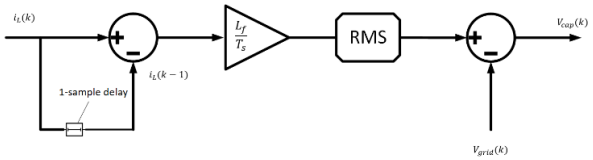

FIGURE 8. Block diagram illustrating the algorithm designed for estimation of the capacitor voltage (DC-bus voltage).

DC-bus voltage and the estimated capacitor voltage (V_{Cap}), given by (8).

To carry out the Current Derivative Calculation, presented in block {26} of Figure 6, the mathematical analysis begins with the estimation of the capacitor voltage.

Rewriting $di_L(t)/d_t$ in function of discrete samples, it is possible to obtain a difference equation for digital control implementation of V_{Cap} estimation. Computational derivative calculation depends on the choosing of the correct measuring window. In order to improve resolution and provide reliability in the task of capacitor voltage estimation, the measuring window is equal to the sampling period. In this context, the capacitor voltage is given by (9), where the discrete expression of current derivative is shown. It is important to mention that due to the system's non-idealities (line inductance, inductor filter resistance, and semiconductor losses, for instance) it is possible to verify quantitative differences between the estimated and the real value. In order to compensate the losses effects in the voltage prediction, it was adopted a proportional gain (K_p) that can be obtained experimentally. Figure 8 shows a block diagram illustrating the algorithm designed for estimation of the V_{Cap} (DC-bus voltage) following the concepts developed from (8) to (10).

$$V_{Cap} = V_{grid} + Lf\frac{di_{Lf}(t)}{dt} \tag{8}$$

$$V_{Cap} = K_p[V_{grid} + Lf.rms\left(\frac{(i_{L_f}(k) - i_{L_f}(k-1))}{T_s}\right)] \tag{9}$$

The value of V_{Cap} can be used to perform the control of the DC-bus voltage in order to guarantee the maximum power extraction under partial shading conditions. Considering (8), it is also possible to derivate a mathematical relation between the switching period and the value of V_{Cap}. In this sense, isolating Δt in (9) and rewriting it in function of discrete intervals of time and inductor current, one has:

$$\Delta t = \frac{L_f \Delta i_L}{V_{cap} - V_{grid}} \tag{10}$$

Thus, one can conclude that is possible to control the value of the DC-bus voltage as a function of Δt, since V_{grid} and Δi_L are sensed and L is the designed filter inductance. These are implemented by defining four experimental classes of calculated capacitor voltage. The definition of those thresholds is performed experimentally, and it is possible to adjust them to guarantee the MPPT according to the design specifications. For this project, four different temperatures were chosen (25°C, 40°C, 55°C and 70°C) and for them the Vmp was defined in order to determinate the estimated capacitor voltage (Vcap) for these temperatures. Then, applying (10), their respective HFSTP were calculated and latter experimentally adjusted to define the operating zones presented in Table 1. It can be noticed that, as expected from (10), the closer are Vcap and Vgrid values, the higher the HFSPT.

IV. RESULTS AND DISCUSSIONS

To show the accuracy of the proposed GMPPT technique, both simulation and experimental tests were carried out. Firstly, it was simulated using PSIM® and the control algorithm was implemented using the C-block function. Later, the control algorithm was embedded in TI Digital Signal Processor (DSP) TMS320F28335 and a 1.0 kW laboratory prototype was implemented to obtain experimental results. Figure 9 shows the system physical structure while Table 2 provides the technical data of its main elements.

A SAS (Solar Array Simulator) was used as the PV array, performing steady state, transient and non-uniform irradiance conditions. The performance of the proposed GMPPT

TABLE 1. Chosen HFSPT in function of the estimated capacitor voltage.

Estimated Capacitor Voltage	HFSPT	PV array temperature range
>260V	161µs	25º
245V - 260V	181µs	25º - 40º
230V - 245V	241µs	40º - 55º
200V - 230V	761µs	>70º

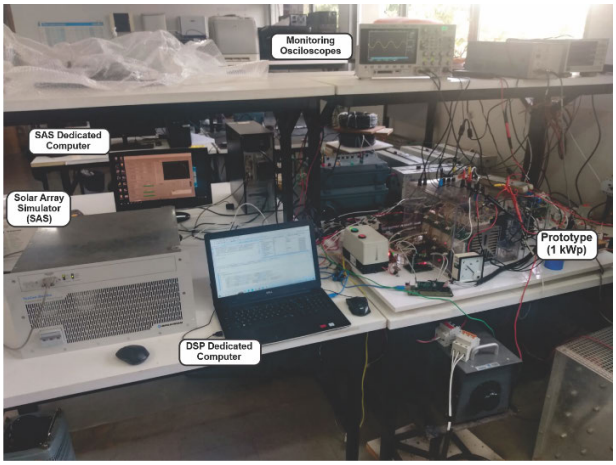

FIGURE 9. Experimental laboratory setup.

technique under steady state operation was analyzed for an irradiance range from 400 W/m^2 to 1000 W/m^2 and temperature range from 25 °C to 70 °C, combining all the aforementioned cases. Using the SAS it is possible to observe both PV array curves (I-V and P-V) and real-time parameters such as: operating voltage, operating current, operating power, as well their maximum e minimum values. Hence, it is also possible to evaluate the accuracy of the MPPT technique through real time calculation of the TF (Tracking Factor), as can be seen in Figs. 10 and 12.

TABLE 2. Prototype technical data.

	Component	Specification
Full-Bridge DC-AC Converter	Capacitor C_{Bus}	Electrolytic 3,3 mF, 900 V
	Inverter Module SEMIKRON	IGBT switches 2 kVA, 500 V
	Switching Frequency	<15 kHz
	Inductor L_f	Silicon steel toroidal core 10 mH
Microprocessor	DSP TMS320F28335	*Clock*: 150 MHz; GPIO: 176; A/D Converter: 80ns; RAM: 68 kB
Power Supply	Solar Array Simulator (SAS)	REGATRON TopCon TC 10 kW
PV Array Model	Pmax; Vmp; Imp; Voc; Isc	1018 W; 265.5 V; 3.77 A; 331.5 V; 4.2 A

A. EXPERIMENTAL ANALYSIS UNDER UNIFORM AND TRANSIENT IRRADIANCE CONDITION

Figure 10 shows the most significant variables and parameters for the steady state response in the standard-test conditions (STC – 25 °C and 1000 W/m^2). Figure 10(a) shows the SAS screen were the nominal parameters of the prototype can be observed, with a nominal power of 1 kW, Maximum Power Point Voltage (V_{MP}) of 265.2 V, and Maximum Power Point Current (I_{MP}) of 3.77 A. It also shows the average bus voltage is 263.55 V, with a deviation of 0.6% from V_{MP}, and the average current at 3.775 A, with a deviation of 0.1% from I_{MP}. In addition, it shows the high TF the proposed technique, achieving 99.45% in nominal operation.

Figure 10(b) illustrates V_{Bus} (or PV array voltage), V_g (grid voltage) and grid injected current i_{Lf}, with an average V_{PV} of 264 V (close of the ideal point of 265.2 V) and average i_{Lf} current injected of 7.1A. Figure 10(c) shows the total harmonic distortion (THD) for the STC and the odd harmonic spectrum of the current injected into the grid. Both THDi and PF (power factor) were compared to what the IEEE 1547/2008 standards define [21]. With a power factor higher than the 0.94 limit and the calculated THD_I in 3.82%, one can be note that the limits were respected.

Figure 11 shows the results of the proposed technique operating under transient irradiance conditions. In Figure 11(a), the SAS provides a irradiance variation from 1000 W/m^2 to 400 W/m^2 over a 2-second ramp. It can be observed that both the DC bus voltage (V_{bus}) and the inject current (i_{Lf}) present a good transient response once the system stabilizes after 600 ms, which is low and does not compromise the energy yield. It is also worth noting the small negative overshoot of the DC bus voltage (4%), reinforcing the system stability. In Figure 11(b), the system initially operates with 400 W/m^2 increasing to 1000 W/m^2 over a 2-second ramp. In this case, V_{bus} rises with bigger overshoot during the irradiance variation, causing the settling time to be slower than in the previous case, taking approximately 2.8 seconds to stabilize. In both cases, despite the slower settling time when compared to other techniques such as proposed in [17], [22], and [23], it does not compromise the system's energy yield since the static and dynamic accuracy of the proposed SPVAVC-GMPPT algorithm is kept around 99% as desired. Finally, Table 3 presents the results obtained for all experimental and simulation tests mentioned above, under different conditions of both irradiance and temperature. It is important to highlight that in all tested conditions, the TF remained above 99%, proving the effectiveness of the proposed technique.

B. EXPERIMENTAL ANALYSIS UNDER NON-UNIFORM IRRADIANCE CONDITION

The SAS platform also performs transient and non-uniform irradiance conditions tests, enabling variations in both irradiance and temperature for the emulated PV array. Hence, partial shading tests were also performed and analyzed to

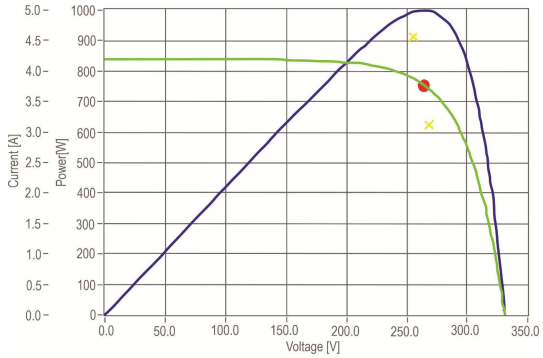

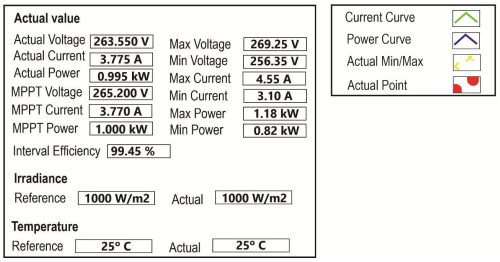

(a)

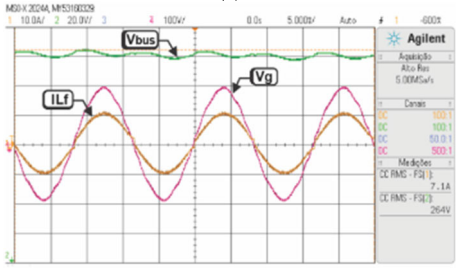

(b)

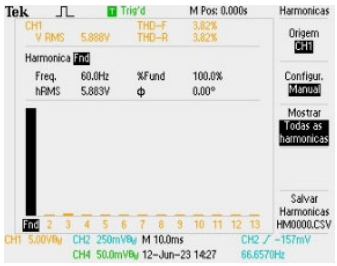

(c)

FIGURE 10. Experimental results obtained under uniform irradiance condition: (a) SAS configuration for PV array emulation in STC (b) inverter's waveforms of V_{bus}, i_{Lf} and V_g (c) harmonic spectrum of the injected current.

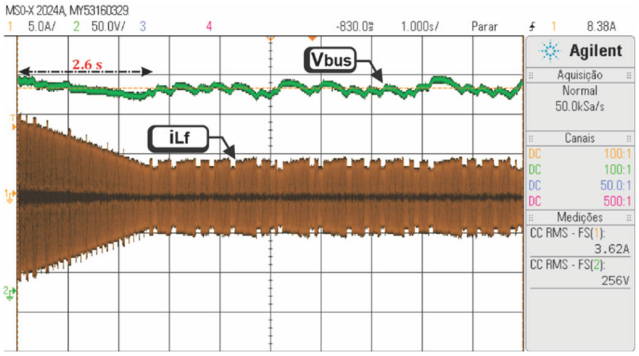

(a)

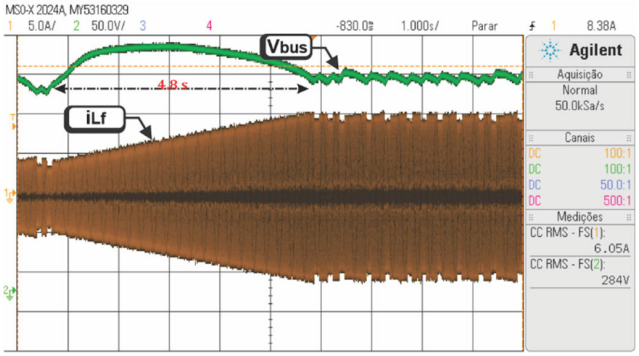

(b)

FIGURE 11. Experimental results obtained under conditions of irradiance ramp variation at constant temperature of 25°C: (a) irradiance reduction from 1000 W/m^2 to 400 W/m^2 (b) irradiance increase from 400 W/m^2 to 1000 W/m^2.

TABLE 3. Summary of experimental results.

Temperature [ºC]	Irradiance [W/m^2]	Vpv [V]	Ipv [A]	TF (Exp) [%]	TF (Sim) [%]
25	1000	263.55	3.775	99.45	99.78
	800	262.80	3.040	99.78	99.62
	600	260.10	2.300	99.63	99.61
	400	252.80	1.550	99.33	99.69
40	1000	256.95	3.705	99.61	99.60
	800	248.10	3.085	99.90	99.13
	600	250.05	2.290	99.79	99.51
	400	243.15	1.545	99.92	99.58
55	1000	238.20	3.810	99.96	99.68
	800	232.95	3.120	99.73	99.27
	600	225.75	2.385	99.31	99.70
	400	225.00	1.585	99.50	99.52
70	1000	223.80	3.845	99.67	99.77
	800	218.70	3.155	99.79	99.20
	600	216.60	2.380	99.60	99.72
	400	213.30	1.585	99.50	99.45

validate the GMPPT proposed technique. To perform the partial shading test, the P-V curve was generated using PSIM software. Then, the correspondent data points were saved and used as input for the SAS, generating the I-V and P-V curves shown in Fig. 12. One can observe that the P-V curve presents two FMPPs, one at 602 W (Vmp = 161V and Imp = 3,74 A) and another at 595W (Vmp = 290V and Imp = 2,05 A) and one GMPP at 710 W ((Vmp = 219V and Imp = 3,26 A). In Fig. 12 one can see that the system operates on the GMPP. Finally, Fig. 13 illustrates DC-bus voltage V_{Bus}, gird voltage V_g and the injected current i_{Lf}, with an average V_{PV} of 217 V (with a voltage deviation of -0,91% from the GMPP at 219 V) and average i_{Lf} injected current of 5.29A.

C. SIMULATION ANALYSIS UNDER IRRADIANCE SEVERE TRANSIENT CONDITION

In order to demonstrate the effectiveness of the proposed control strategy under severe irradiance variation conditions (step variation) simulation tests were also conducted. Under these operating conditions, experimental tests were not carried out

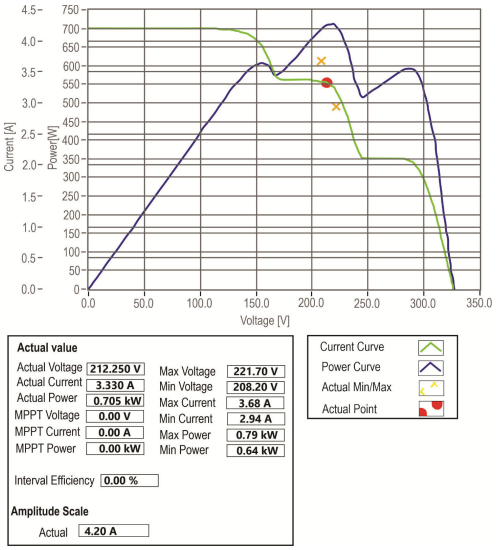

FIGURE 12. Non-uniform solar irradiance test condition: I-V and P-V curves reproduced with SAS used to supply the grid-tied inverter.

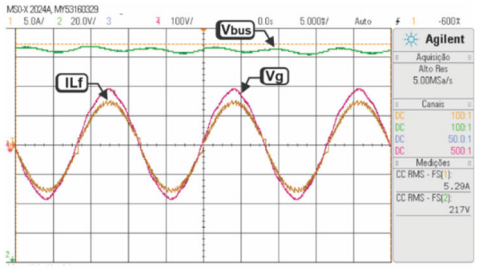

FIGURE 13. Non-uniform solar irradiance test condition: corresponding time signals of V_{bus}, I_{Lf} and V_g at the GMPP (illustrated in Fig. 12).

in order to avoid situations in which, considering the experimental laboratory setup available, there could be a reverse power flow (from AC side to the SAS) due to intense DC-bus voltages oscillations and, consequently, damage to the equipment.

That being sad, Fig. 14 presents simulation results for an initial irradiance condition of 1000 W/m^2 at 25 °C submitted to a negative step of 600 W/m^2. In Fig. 14(a), from top to bottom, irradiance, tracking factor (TF), and the peak reference of the injected current are presented. In Fig. 14(b), are presented the photovoltaic array voltage (V_{PV}) and the injected current (i_{Lf}). It can be observed a 3-second settling time for the system under an extreme irradiance variation. During the transient condition, V_{PV} voltage drops close to 150V so the injected current is decreased making it possible to reestablish the V_{PV} voltage at around 250 V after 3 seconds. Hence, the injected current reference is increased again in search of the MPP, as expected.

Figure 15 presents for an initial irradiance condition of 400 W/m^2 at 25 °C submitted to a positive step of 600 W/m^2. In Figure 15(a), irradiance is presented again

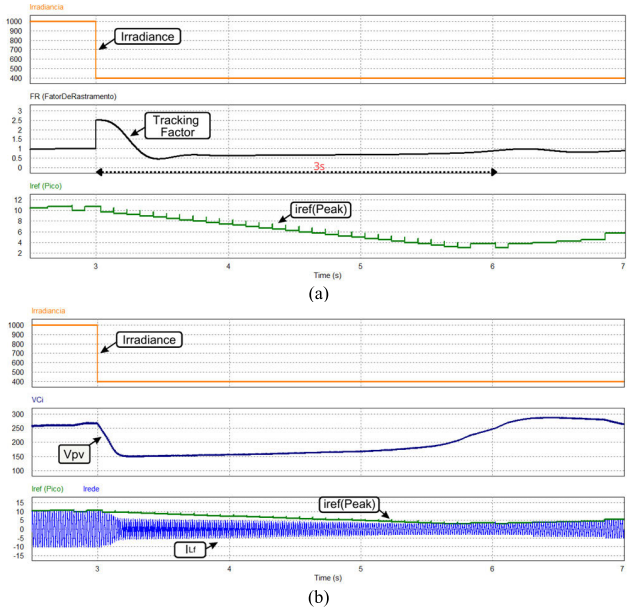

FIGURE 14. Simulation results under irradiance severe transient condition from 1000 W/m^2 to 400 W/m^2: (a) corresponding signals of irradiance, TF and current control reference (b) corresponding signals of Vpv and I_{Lf}.

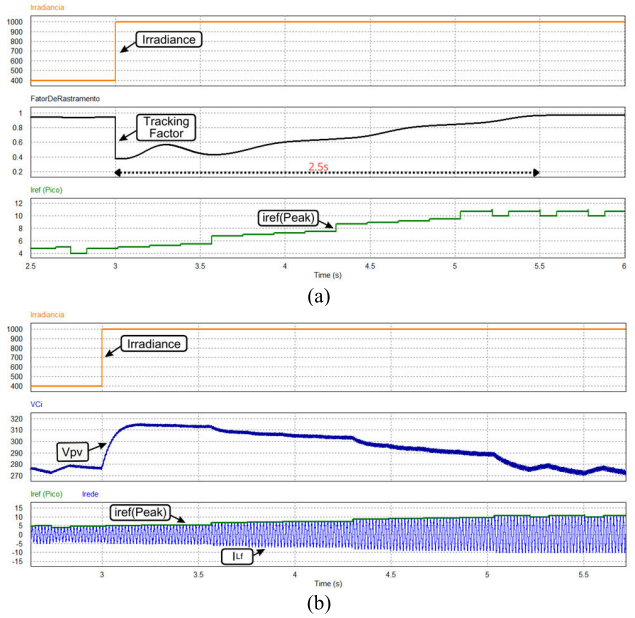

FIGURE 15. Simulation results under irradiance severe transient condition (from 400W/m^2 to 1000W/m^2): (a) corresponding signals of irradiance, TF and current control reference (b) corresponding signals of Vpv and I_{Lf}.

(with the moment of its step), the tracking factor, and the peak reference of injected current. In Figure 14(b), the photovoltaic array voltage and the injected current are also shown. It can be observed a 2.5-second settling time for the system under an extreme irradiance variation of 600 W/m^2. Soon after the increase in irradiance, V_{PV} increases, and the injected current reference begins to increase seeking the new MPP and causing a correspondent reduction in V_{PV}. As expected,

V_{PV} is controlled indirectly through disturbances imposed on the injected current reference, causing the system to operate at MPP. The results indicate settling time of around 3 seconds, confirming the control strategy's ability to respond to dynamic irradiance changes reasonably fast and not compromising the energy harvest since the operation at the MPP is assured with TF over 99%.

V. CONCLUSION

This paper presents the study regarding the development of a single-stage single-phase grid-tied photovoltaic (PV) inverter with a new Global Maximum Power Point Tracking (GMPPT) technique. The proposed strategy is based on the indirect PV Array Voltage Control and allows for the development of PV inverter with reduced number of sensors, therefore, increasing the system reliability and reducing costs. The proposed strategy was denominated as Sensorless PV Array Voltage Control for Global Maximum Power Point Tracking (SPVAVC-GMPPT).

The new algorithm does not require full scanning of the output power curve so that the GMPP can be reached and does not require subroutines to determine the desired injected current reference, reducing both the complexity of the control strategy and the losses in the energy harvest.

Experimental results demonstrate the effectiveness of the proposed control strategy under different irradiance and temperature conditions achieving a Tracking Factor over 99% TF converging to the Global Maximum Power Point (GMPP) even non-uniform irradiance conditions.

REFERENCES

[1] Y. Zhao, R. Ball, J. Mosesian, J.-F. de Palma, and B. Lehman, "Graph-based semi-supervised learning for fault detection and classification in solar photovoltaic arrays," *IEEE Trans. Power Electron.*, vol. 30, no. 5, pp. 2848–2858, May 2015, doi: 10.1109/TPEL.2014.2364203.

[2] S. Makhloufi and S. Mekhilef, "Logarithmic PSO-based global/local maximum power point tracker for partially shaded photovoltaic systems," *IEEE J. Emerg. Sel. Topics Power Electron.*, vol. 10, no. 1, pp. 375–386, Feb. 2022, doi: 10.1109/JESTPE.2021.3073058.

[3] J. Ahmed and Z. Salam, "A critical evaluation on maximum power point tracking methods for partial shading in PV systems," *Renew. Sustain. Energy Rev.*, vol. 47, pp. 933–953, Jul. 2015, doi: 10.1016/j.rser.2015.03.080.

[4] J. P. Ram, T. S. Babu, and N. Rajasekar, "A comprehensive review on solar PV maximum power point tracking techniques," *Renew. Sustain. Energy Rev.*, vol. 67, pp. 826–847, Jan. 2017, doi: 10.1016/j.rser.2016.09.076.

[5] N. A. Kamarzaman and C. W. Tan, "A comprehensive review of maximum power point tracking algorithms for photovoltaic systems," *Renew. Sustain. Energy Rev.*, vol. 37, pp. 585–598, Sep. 2014, doi: 10.1016/j.rser.2014.05.045.

[6] M. Chen, S. Ma, J. Wu, and L. Huang, "Analysis of MPPT failure and development of an augmented nonlinear controller for MPPT of photovoltaic systems under partial shading conditions," *Appl. Sci.*, vol. 7, no. 1, p. 95, Jan. 2017, doi: 10.3390/app7010095.

[7] Z. Salam, J. Ahmed, and B. S. Merugu, "The application of soft computing methods for MPPT of PV system: A technological and status review," *Appl. Energy*, vol. 107, pp. 135–148, Jul. 2013, doi: 10.1016/j.apenergy.2013.02.008.

[8] M. Seyedmahmoudian, B. Horan, T. K. Soon, R. Rahmani, A. M. T. Oo, S. Mekhilef, and A. Stojcevski, "State of the art artificial intelligence-based MPPT techniques for mitigating partial shading effects on PV systems—A review," *Renew. Sustain. Energy Rev.*, vol. 64, pp. 435–455, Oct. 2016, doi: 10.1016/j.rser.2016.06.053.

[9] A. Ali, K. Almutairi, S. Padmanaban, V. Tirth, S. Algarni, K. Irshad, S. Islam, M. H. Zahir, M. Shafiullah, and M. Z. Malik, "Investigation of MPPT techniques under uniform and non-uniform solar irradiation Condition-A retrospection," *IEEE Access*, vol. 8, pp. 127368–127392, 2020, doi: 10.1109/ACCESS.2020.3007710.

[10] N. Karami, N. Moubayed, and R. Outbib, "General review and classification of different MPPT techniques," *Renew. Sustain. Energy Rev.*, vol. 68, pp. 1–18, Feb. 2017, doi: 10.1016/j.rser.2016.09.132.

[11] S. H. Hanzaei, S. A. Gorji, and M. Ektesabi, "A scheme-based review of MPPT techniques with respect to input variables including solar irradiance and PV arrays' temperature," *IEEE Access*, vol. 8, pp. 182229–182239, 2020, doi: 10.1109/ACCESS.2020.3028580.

[12] B. N. Alajmi, K. H. Ahmed, S. J. Finney, and B. W. Williams, "Fuzzy-logic-control approach of a modified hill-climbing method for maximum power point in microgrid standalone photovoltaic system," *IEEE Trans. Power Electron.*, vol. 26, no. 4, pp. 1022–1030, Apr. 2011, doi: 10.1109/TPEL.2010.2090903.

[13] S. R. Devireddy, S. Porpandiselvi, and B. Salvi, "A GMPPT algorithm for PV systems using current reference and P-I curve under partial shading conditions," in *Proc. IEEE Int. Conf. Power Electron., Smart Grid, Renew. Energy (PESGRE)*, Trivandrum, India, Jan. 2022, pp. 1–6, doi: 10.1109/PESGRE52268.2022.9715816.

[14] M. Boztepe, F. Guinjoan, G. Velasco-Quesada, S. Silvestre, A. Chouder, and E. Karatepe, "Global MPPT scheme for photovoltaic string inverters based on restricted voltage window search algorithm," *IEEE Trans. Ind. Electron.*, vol. 61, no. 7, pp. 3302–3312, Jul. 2014, doi: 10.1109/TIE.2013.2281163.

[15] N. M. Elbehairy, R. A. Swief, A. M. Abdin, and T. S. Abdelsalam, "Maximum power point tracking for a stand alone PV system under shading conditions using flower pollination algorithm," in *Proc. 21st Int. Middle East Power Syst. Conf. (MEPCON)*, Cairo, Egypt, Dec. 2019, pp. 840–845, doi: 10.1109/MEPCON47431.2019.9008230.

[16] D. Cortes-Vega, H. Alazki, and J. L. Rullan-Lara, "Current sensorless MPPT control for PV systems based on robust observer," *Appl. Sci.*, vol. 12, no. 9, p. 4360, Apr. 2022, doi: 10.3390/app12094360.

[17] P. A. R. Freitas, L. P. Pires, L. C. Freitas, G. B. Lima, and L. C. G. Freitas, "Design and development of a grid-tied PV inverter with GMPPT technique and reduced number of sensors," *IEEE Access*, vol. 10, pp. 48810–48823, 2022, doi: 10.1109/ACCESS.2022.3172404.

[18] M. Alqatamin and M. L. McIntyre, "Nonlinear self-synchronizing current control for grid-connected photovoltaic inverters," *Energies*, vol. 15, no. 13, p. 4855, Jul. 2022, doi: 10.3390/en15134855.

[19] B. Chen, B. Gu, J. S. Lai, and W. Yu, "A high efficiency and reliability single-phase photovoltaic micro-inverter with high magnetics utilization for nonisolated AC-module applications," in *Proc. IEEE Energy Convers. Congr. Expo.*, Sep. 2013, pp. 2406–2411.

[20] M. E. T. Souza, E. C. Resende, F. C. Melo, G. B. de Lima, and L. C. G. de Freitas, "Computational implementation and comparative analysis of phase-locked loop (PLL) methods under different power quality disturbances," in *Proc. IEEE PES Innovative Smart Grid Technol. Conf.*, Gramado, Brazil, 2019, pp. 1–6, doi: 10.1109/ISGT-LA.2019.8894920.

[21] *IEEE Recommended Practice for Utility Interface of Residential and Intermediate Photovoltaic (PV) Systems*, Standard ANSI/IEEE Std 929-1988, Nov. 1987, doi: 10.1109/IEEESTD.1987.79148.

[22] M. Kermadi, Z. Salam, J. Ahmed, and E. M. Berkouk, "A high-performance global maximum power point tracker of PV system for rapidly changing partial shading conditions," *IEEE Trans. Ind. Electron.*, vol. 68, no. 3, pp. 2236–2245, Mar. 2021, doi: 10.1109/TIE.2020.2972456.

[23] S. Mohanty, B. Subudhi, and P. K. Ray, "A new MPPT design using grey wolf optimization technique for photovoltaic system under partial shading conditions," *IEEE Trans. Sustain. Energy*, vol. 7, no. 1, pp. 181–188, Jan. 2016, doi: 10.1109/TSTE.2015.2482120.

[24] M. X. Bui, M. Faz Rahman, D. Guan, and D. Xiao, "A new and fast method for on-line estimation of D and Q axes inductances of interior permanent magnet synchronous machines using measurements of current derivatives and inverter DC-bus voltage," *IEEE Trans. Ind. Electron.*, vol. 66, no. 10, pp. 7488–7497, Oct. 2019, doi: 10.1109/TIE.2018.2883274.

[25] S. Padmanaban, N. Priyadarshi, J. B. Holm-Nielsen, M. S. Bhaskar, F. Azam, A. K. Sharma, and E. Hossain, "A novel modified sine-cosine optimized MPPT algorithm for grid integrated PV system under real operating conditions," *IEEE Access*, vol. 7, pp. 10467–10477, 2019, doi: 10.1109/ACCESS.2018.2890533.

PEDRO A. R. FREITAS was born in Uberlândia, Minas Gerais, Brazil, in 1990. He received the B.S. and master's degrees in electrical engineering from the Federal University of Uberlândia (UFU), in 2012 and 2014, respectively, where he is currently pursuing the Ph.D. degree in power electronics. In 2014, he joined the Federal Institute of the Triângulo Mineiro, IFTM, where he is also a Professor. His research interests include photovoltaic systems and sustainable energies.

LUCAS P. PIRES was born in Catalão, Goiás, Brazil, in 1992. He received the Graduate degree from the Federal University of Triângulo Mineiro (UFTM), in 2014, the master's degree from the Federal University of Uberlândia (UFU), in 2016, with a dissertation in the area of bidirectional inverters applied to direct current microgrids, and the Ph.D. degree in electrical engineering from UFU, in 2019, with a thesis linked to the development of a new strategy for extracting maximum power for photovoltaic modules connected to the electricity grid. He is currently an Electrical Engineer with UFTM, where he is also a Professor. He is also a collaborating Researcher with the Research Center in Power Electronics (NUPEP), UFU. His research interests include renewable energies with an emphasis on solar technology, techniques for extracting maximum power from photovoltaic modules, bidirectional power converters, electric vehicles, and control applied to power electronics.

LUIZ C. FREITAS was born in Monte Alegre, Minas Gerais, Brazil, in April 1952. He received the M.Sc. and Ph.D. degrees in power electronics from the Federal University of Santa Catarina, Florianópolis, Brazil, in 1985 and 1992, respectively. In 1991, he founded the Research Center in Power Electronics, Federal University of Uberlândia (UFU). He has authored a variety of papers particularly in the areas of soft switching, DC–DC, DC–AC, and AC–DC converters. He has published in PESC-92, APEC-93, PESC-93, and IEEE TRANSACTIONS ON POWER ELECTRONICS, in January 1995, a family of soft-switching converters that promote the driving input and output of switches with zero voltage, which, since then, he has been widely used in research related to non-dissipative switching converters. Since 1996, he has been a Researcher recognized by the National Council for Scientific and Technological Development (CNPq) with a Research Productivity Grant. He is currently a retired Professor with UFU, where he is a collaborating Researcher with the Postgraduate Program, Faculty of Electrical Engineering. He has more than 79 articles published in national and international journals, and more than 244 papers published in conferences. His research interests include the design and development of power electronics converters.

ÊNIO C. RESENDE received the Graduate degree in electrical engineering from the Federal University of Uberlândia (UFU), Brazil, with an exchange period through the CsF/CAPES Program with Sacramento State University (SAC-State), Sacramento, CA, USA, in 2018, and the M.Sc. degree in electrical engineering with the specialization in power electronics from the Power Electronics Research Center (NUPEP), UFU Postgraduate Program, in 2020, where he is currently pursuing the Ph.D. degree in electrical engineering. During the master's degree, he studied and developed islanding detection techniques, synchronization strategies, and MPPT methods. His research interests include islanding detection, distributed generation, renewable energies, MPPT, control methods, and power quality.

HENRIQUE T. DE M. CARVALHO received the B.Sc. degree in electrical engineering and the M.Sc. degree in electrical engineering—power electronics from the Federal University of Uberlândia (UFU), Uberlândia, Brazil, in 2016 and 2019, respectively, where he is currently pursuing the Ph.D. degree in electrical engineering—power electronics. His research interests include the distributed control of AC microgrids, the design and control of grid-connected inverter, and power electronics solutions for renewable energy and smart power systems.

LUIZ C. G. FREITAS was born in Uberlândia, Brazil, in 1976. He received the Graduate degree in electrical engineering with emphasis on power systems and the master's and Ph.D. degrees in electrical engineering with emphasis on power electronics from the Federal University of Uberlândia (UFU), in 2001, 2003, and 2006, respectively. In his doctoral thesis, he developed an innovative topological design of a three-phase hybrid rectifier for high power drive systems. In 2012, he received the Second Prize Paper Award of the IEEE-IAS-Industrial Automation and Control Committee (IACC) for his contribution to the development of hybrid rectifier structures. In 2008, he joined as a Faculty Member of UFU, where he is currently developing teaching and research activities in the area of power electronics and power systems. Since 2010, he has been the Coordinator of the Power Electronics Research Center (NUPEP), Faculty of Electrical Engineering, UFU. Since 2013, he has been a Researcher recognized by the National Council for Scientific and Technological Development (CNPq) with a Research Productivity Grant. His research interests include electrical engineering, conversion and rectification of electric energy, working on various topics related to power electronics, electrical power quality, and renewable energy.

GUSTAVO B. LIMA was born in Ibiassucê, Brazil, in 1986. He received the B.Sc., M.Sc., and Ph.D. degrees in electrical engineering from the Federal University of Uberlândia (UFU), Uberlândia, Minas Gerais, Brazil, in 2010, 2012, and 2015, respectively. In 2017, he joined as a Faculty Member of UFU, where he is currently developing teaching and research activities in the area of power electronics and power systems as a member of the Power Electronics Research Center (NUPEP), Faculty of Electrical Engineering, UFU. His research interests include hybrid rectifiers, digital control applied to power electronics, and power factor correction.